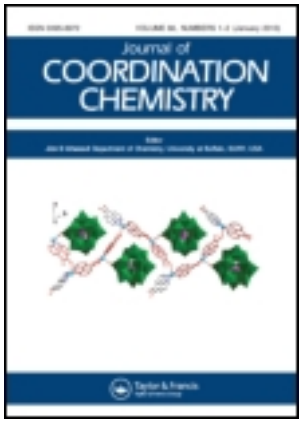

Journal of Coordination Chemistry
Publication details, including instructions for authors and subscription information:
http://www.tandfonline.com/loi/gcoo20

Copper(II) complex of monobasic tridentate ONN donor ligand: synthesis, encapsulation in zeolite-Y, characterization, and catalytic activity

Mannar R. Maurya [a], Chanchal Haldar [a], Shilpa Behl [b], NareshBabu Kamatham [a] & Fernando Avecilla [c]

[a] Department of Chemistry, Indian Institute of Technology Roorkee, Roorkee 247 667, India

[b] CET-IILM, Academy of Higher Learning, KP-II, Greater Noida, Uttar Pradesh 201306, India

[c] Departamento de Química Fundamental, Universidade da Coruña, Campus de A Zapateira, 15071A Coruña, Spain

Published online: 07 Sep 2011.

To cite this article: Mannar R. Maurya, Chanchal Haldar, Shilpa Behl, NareshBabu Kamatham & Fernando Avecilla (2011) Copper(II) complex of monobasic tridentate ONN donor ligand: synthesis, encapsulation in zeolite-Y, characterization, and catalytic activity, Journal of Coordination Chemistry, 64:17, 2995-3011, DOI: 10.1080/00958972.2011.610450

To link to this article: http://dx.doi.org/10.1080/00958972.2011.610450

Journal of Coordination Chemistry
Vol. 64, No. 17, 10 September 2011, 2995–3011

Copper(II) complex of monobasic tridentate ONN donor ligand: synthesis, encapsulation in zeolite-Y, characterization, and catalytic activity

MANNAR R. MAURYA*†, CHANCHAL HALDAR†, SHILPA BEHL‡, NARESHBABU KAMATHAM† and FERNANDO AVECILLA§

†Department of Chemistry, Indian Institute of Technology Roorkee, Roorkee 247 667, India
‡CET-IILM, Academy of Higher Learning, KP-II, Greater Noida, Uttar Pradesh 201306, India
§Departamento de Química Fundamental, Universidade da Coruña, Campus de A Zapateira, 15071A Coruña, Spain

(*Received 8 March 2011; in final form 8 July 2011*)

Reaction between $CuCl_2$ and (Z)-2-(1-(2-(1H-benzo[d]imidazol-2-yl)ethylimino)ethyl)phenol (Hhap-aebmz) derived from *o*-hydroxyacetophenone (Hhap) and 2-aminoethylbenzimidazole (aebmz) gives [Cu^{II}(hap-aebmz)Cl]. Elemental analysis, magnetic susceptibility, spectral (IR and electronic) data, and single crystal X-ray studies confirm the distorted square planar structure of the complex. [Cu^{II}(hap-aebmz)Cl] has been encapsulated in the nano-cavity of zeolite-Y and its encapsulation is ensured by various physico-chemical techniques. The encapsulated complex has been used as a catalyst for oxidation of cyclohexene and phenol in the presence of H_2O_2. With nearly quantitative oxidation of cyclohexene, the selectivity of the oxidation products follows the order, 2-cyclohexene-1-ol (44%) > 2-cyclohexene-1-one (40%) > cyclohexeneoxide (12%) > cyclohexane-1,2-diol (4%). Oxidation of phenol (65.7%) gives catechol (66.1%) > hydroquinone (32.9%).

Keywords: Crystal structure; Zeolite-Y; [Cu^{II}(hap-aebmz)Cl]-Y; Catalyst; Oxidation of cyclohexene; Oxidation of phenol

1. Introduction

Coordination chemistry of monobasic tridentate ONN ligands has been studied due to their interesting structural, magnetic, and other properties [1–8]. One coordination site of such ligands can be involved in bridging with other metal centers producing dinuclear or polynuclear species [1–8]. Dimerization through X bridging in complexes of formula [MLX] (M = Cu^{II}, Ni^{II}, Zn^{II}, Mn^{III}, Cd^{II}, etc., L = ONN monobasic tridentate ligands and X = N_3^-, Cl^-, NCO^-, NCS^-, etc.) are also known [4–8]. Mononuclear complexes, in the presence of suitable oxidant, may expand the coordination number, facilitating

*Corresponding author. Email: rkmanfcy@iitr.ernet.in

Journal of Coordination Chemistry
ISSN 0095-8972 print/ISSN 1029-0389 online © 2011 Taylor & Francis
DOI: 10.1080/00958972.2011.610450

catalytic oxidation. We earlier prepared mononuclear complexes [$V^{V}O_2$(sal-ambmz)] and [Cu^{II}(sal-ambmz)Cl] and encapsulated them in the nano-cavity of zeolite-Y, and studied their catalytic properties [9]. Such zeolite encapsulated metal complexes (ZEMC) have provided the opportunity to develop catalytic processes for selective oxidation of various substrates and are able to produce important intermediates [10–15]. In this article, we report the mononuclear copper(II) complex of (Z)-2-(1-(2-(1H-benzo[d]imidazol-2-yl)ethylimino)ethyl)phenol (Hhap-aebmz, **I**; scheme 1), its characterization by single crystal X-ray study and encapsulation in the nano-cavity of zeolite-Y. Catalytic activities of encapsulated complex have been studied for oxidation of cyclohexene and phenol and compared with the corresponding neat analog.

2. Experimental

2.1. *Material and methods*

All chemicals and solvents were of AR grade and used without purifications. Elemental analyses of the ligand and complex were obtained with an Elementar model Vario-EL-III. Copper content in the zeolite-Y complex was obtained by Atomic Absorption Spectroscopy. IR spectra were recorded as KBr pellets on a Nicolet NEXUS Aligent 1100 FT-IR spectrometer after grinding the sample with KBr. Electronic spectra of ligand and complex were recorded in methanol on a Shimadzu 1601 PC UV–VIS spectrophotometer. Electronic spectrum of zeolite-Y encapsulated complex was recorded in Nujol by layering the mull of the sample inside one of the cuvettes while keeping the other one layered with Nujol as reference. ^{1}H NMR and ^{13}C NMR spectra were obtained in $CDCl_3$ on a Bruker Avance III 400 MHz spectrometer with the common parameter settings. The magnetic susceptibility of the complex was measured at 298 K with vibrating sample magnetometer model 155, using nickel metal with saturation magnetization of 55 emu g^{-1} as standard. X-ray powder diffractograms of zeolite related samples were recorded using a Bruker AXS D8 advance X-ray powder diffractometer with a Cu-Kα target. Scanning electron micrograph (SEM) of zeolite-Y having encapsulated complex was recorded on a Leo instrument model 435VP. Energy dispersive X-ray analysis (EDX) was obtained on a FEI Quanta 200 FEG. The sample was dusted on alumina and coated with a thin film of gold to prevent surface charging and to protect the surface material from thermal damage by the electron beam. In all analyses, a uniform thickness of about 0.1 mm was maintained.

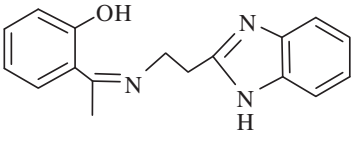

Scheme 1. Structure of (Z)-2-(1-(2-(1H-benzo[d]imidazol-2-yl)ethylimino)ethyl)phenol (Hhap-aebmz, **I**).

2.2. *Preparations*

2.2.1. Preparation of Hhap-aebmz (I). An aqueous solution of aebmz · 2HCl (4.680 g, 20 mmol in 15 mL water) was neutralized by adding aqueous Na_2CO_3 solution (2.120 g, 20 mmol). A methanolic solution of *o*-hydroxyacetophenone (2.72 g, 20 mmol in 20 mL) was added dropwise to the above solution with stirring. A yellow solid slowly separated from the solution within 2 h, was filtered, washed thoroughly with water followed by petroleum ether and dried in vacuum at room temperature. Finally it was recrystallized from acetonitrile. Yield: 4.24 g (75.9%). Anal. Calcd for $C_{17}H_{17}N_3O$ (279.34) (%): C, 73.1; H, 6.1; N, 15.0. Found (%): C, 72.7; H, 6.2; N, 15.1. ^{1}H NMR ($CDCl_3$, δ/ppm): 7.5(b, 2H, −OH and −NH). 7.47(d, 1H), 7.3(d, 1H), 7.26(s, 2H), 7.19(q, 2H), 6.9(d, 1H), 6.7(t, 1H, aromatic), 4.09(t, 2H, $-CH_2$), 3.38(t, 2H, $-CH_2$), 2.3(s, 3H, $-CH_3$). ^{13}C NMR ($CDCl_3$, δ/ppm): 14.7 (CH_3), 30.4 (CH_2CH_2N), 47.3 (CH_2CH_2N), 152.1 (NH–*C*=N, benzimidazole), 164.8 (ph–*C*–OH), 173.5 (C=N, imine), 117.1, 118.7, 119.0, 122.3, 128.3, 133.3 (aromatic).

2.2.2. Preparation of [Cu^{II}(hap-aebmz)Cl] (1). A solution of $CuCl_2 \cdot 2H_2O$ (0.852 g, 5 mmol) dissolved in methanol (8 mL) was added to a hot solution of Hhap-aebmz (1.396 g, 5 mmol) in methanol (15 mL) and the reaction mixture was stirred for 5 h. The dark green solid of [Cu^{II}(hap-aebmz)Cl] slowly separated, was filtered off, washed with petroleum ether, and dried in vacuum over silica gel. Yield: 1.26 g (67.0 %). Anal. Calcd for $C_{17}H_{16}N_3OClCu$ (377.33) (%): C, 54.1; H, 4.3; N, 11.1. Found (%): C, 53.8; H, 4.4; N, 11.2.

2.2.3. Preparation of [Cu^{II}(hap-aebmz)Cl]-Y (2). A methanolic solution of Hhap-aebmz (2.0 g) was mixed with copper-exchanged zeolite-Y ([Cu^{II}]-Y, 3.0 g) [9] suspended in methanol (50 mL) and the reaction mixture was refluxed for 14 h in an oil bath with stirring. The solid was filtered off, washed with methanol, and again suspended in methanol to remove excess ligand present in the cavities as well as on the surface of the zeolite along with neat complex if any using a Soxhlet extractor. The remaining uncomplexed metal ions in zeolite were removed by stirring with aqueous 0.01 mol L^{-1} NaCl (200 mL) for 8 h. Finally it was washed with doubly distilled water and dried at *ca* 120°C for several hours. Found (%): Cu, 2.4.

2.3. *X-ray crystal structure determination*

3-D X-ray data for Hhap-aebmz (**I**) and [Cu^{II}(hap-aebmz)Cl] (**1**) were collected on a Bruker SMART Apex CCD diffractometer at 100(2) K, using a graphite monochromator and Mo-Kα radiation ($\lambda = 0.71073$ Å) by the ϕ–ω scan method. Reflections were measured from a hemisphere of data collected of frames each covering 0.3° in ω. Of the 14,777 and 26,444 reflections measured, all of which were corrected for Lorentz and polarization effects, and for absorption by semi-empirical methods based on symmetry-equivalent and repeated reflections, 3060 and 3186 independent reflections exceeded the significance level $|F|/\sigma(|F|) > 4.0$. Complex scattering factors were taken from SHELXTL [16]. The structures were solved by direct methods and refined by full-matrix least-squares on F^2. The non-hydrogen atoms were refined with anisotropic

thermal parameters in all cases. Hydrogens were left to refine freely in the two compounds, except H(2N) of the benzimidazole in **I**, which was located from a difference electron density map and fixed to 0.90 to the corresponding heteroatom. A final difference Fourier map showed no residual density outside; minimum and maximum final electron densities: 0.417 and –0.486 for **I** and 0.735 and –0.366 for **1** eÅ^{-3}. Crystal data and details of the data collection and refinement for the new compounds are given in table 1.

2.4. *Catalytic reactions*

2.4.1. Oxidation of cyclohexene. The catalytic reactions were carried out in a glass reactor of 50 mL capacity equipped with a reflux condenser. Cyclohexene (0.82 g, 10 mmol) was dissolved in acetonitrile (5 mL) and to this was added aqueous 30% H_2O_2 (2.27 g, 20 mmol) and [Cu^{II}(hap-aebmz)Cl]-Y (0.005 g). The reaction was carried out in an oil bath with continuous stirring while maintaining the reaction temperature at 80°C. The progress of the reaction was monitored by withdrawing the sample at definite time intervals and analyzing quantitatively through a thermo electron gas chromatograph equipped with HP-1 capillary column (30 × 0.25 mm × 0.25 μm) and FID detector. The identities of the products were confirmed by GC-MS model Perkin-Elmer, Clarus 500 by comparing the fragments of each product with the library available.

2.4.2. Oxidation of phenol. In a typical reaction, aqueous 30% H_2O_2 (2.27 g, 20 mmol) and phenol (1.88 g, 20 mmol) were mixed in 5 mL of acetonitrile and the reaction mixture was heated at 80°C with continuous stirring in an oil bath. [Cu^{II}(hap-aebmz)Cl]-Y

Table 1. Crystal data and structure refinement for (Hhap-aebmz) (**I**) and [Cu^{II}(hap-aebmz)Cl] (**1**).

	I	**1**
Empirical formula	$C_{17}H_{17}N_3O$	$C_{34}H_{32}Cl_2Cu_2N_6O_2$
Formula weight	279.34	754.64
Temperature (K)	100(2)	100(2)
Wavelength (Å)	0.71073	0.71073
Crystal system	Monoclinic	Monoclinic
Space group	*C*2/*c*	$P2_1/c$
Unit cell dimensions (Å, °)		
a	27.9320(9)	8.0432(4)
b	6.5521(2)	10.1802(5)
c	19.5644(6)	18.7209(9)
β	127.6270(10)	99.175(3)
Volume (Å^3), *Z*	2835.80(15), 8	1513.28(13), 2
F(000)	1184	772
Calculated density (g cm^{-3})	1.309	1.656
Absorption coefficient (mm^{-1})	0.084	1.627
Range for data collection (°)	2.63–28.46	2.28–28.41
R_{int}	0.0289	0.0502
Crystal size (mm^3)	0.40 × 0.19 × 0.18	0.35 × 0.12 × 0.09
Goodness-of-fit on F^2	1.083	1.054
R_1[a]	0.0433	0.0322
wR_2 (all data)[b]	0.1204	0.0731
Largest differences peak and hole (e Å^{-3})	0.417 and −0.486	−0.366 and 0.735

[a] $R_1 = \Sigma||F_o| - |F_c||/\Sigma|F_o|$. [b] $wR_2 = \{\Sigma[w(|F_o|^2 - |F_c|^2)^2]/\Sigma[w(F_o^4)]\}^{1/2}$.

(0.010 g) was added to the reaction mixture and the reaction was considered to begin. During the reaction, the products were analyzed and their identities confirmed as mentioned above by withdrawing small aliquots after specific interval of time.

3. Results and discussion

Synthesis of Hhap-aebmz is straightforward. Elemental analysis, IR, ^{1}H, and ^{13}C NMR spectral data, and single crystal X-ray (discussed later) confirm its structure.

Most [Cu^{II}(ONN)X] (where ONN = coordinating atoms of monobasic tridentate ligands, X = Cl^-, Br^-, SCN^-, N_3^-, etc.) complexes exist as dimers/polymers where each unit has square pyramidal structure through X^- bridging [4–8]. The green [Cu^{II}(hap-aebmz)Cl] (**1**), synthesized here by reacting Hhap-aebmz with $CuCl_2$, exists as a monomer with distorted square planar structure (*vide infra*). Magnetic moment of 1.72 μB also suggests its magnetically dilute nature and existence in its monomeric form. Encapsulation of **1** in the nano-cavity of zeolite-Y involved the interaction of [Cu^{II}]-Y with excess Hhap-aebmz in methanol, where ligand slowly enters into the cavity of zeolite-Y due to its flexible nature and interacts with metal ions. Soxhlet extraction using methanol finally purified the impure complex. The remaining uncomplexed metal ions in zeolite were removed by exchanging with aqueous 0.01 mol L^{-1} NaCl solution. As one extra anionic ligand would be required to balance the overall charges on the Cu^{II}, Cl^- of NaCl used during exchanged process fulfills this requirement. The presence of chloride has been confirmed qualitatively. Thus, the formula of Cu^{II} complex may be written as [Cu^{II}(hap-aebmz)Cl]-Y (**2**). As impure **2** was extracted well with methanol, the presence of 2.4% copper is only due to encapsulation of metal complex in the super cages of zeolite-Y. About 10 Å diagonal distance of [Cu^{II}(hap-aebmz)Cl] (**1**) allows its encapsulation in the super cages of zeolite-Y without strain. Similarity in the spectral properties of neat as well as encapsulated complex (*vide infra*) suggests a similar distorted square planar structure for encapsulated complex as well.

3.1. *Description of structures of Hhap-aebmz (I) and [Cu^{II}(hap-aebmz)Cl] (1)*

Light orange crystals of Hhap-aebmz (**I**) were grown by slow evaporation of methanolic solution at room temperature. Figure 1 shows ORTEP representation of Hhap-aebmz (**I**). Table 2 presents bond lengths and angles while table S1 (see Supplementary material) provides distances and angles of hydrogen bonds. Description of structure is given in Supplementary material.

[Cu^{II}(hap-aebmz)Cl] was grown by slow evaporation of methanolic solution at room temperature. The ORTEP plot of the complex is shown in figure 2. The polyhedron is a much distorted square plane. Phenolic oxygen, azomethine nitrogen, benzimidazolic nitrogen, and Cl^- constitute the distorted square plane. Mean deviation from planarity of the plane containing the four donors amounts to 0.4685(9) Å (figure 3). All atoms coordinated to Cu(II) are within 1.9–2.2 Å. Angles O(1)–Cu(1)–N(1): 91.44(7)°; N(1)–Cu(1)–N(2): 89.74(7)°; O(1)–Cu(1)–Cl(1): 92.41(5)°, and N(2)–Cu(1)–Cl(1): 97.75(5)° are close to expected 90°. Selected bond lengths and angles for the complex are

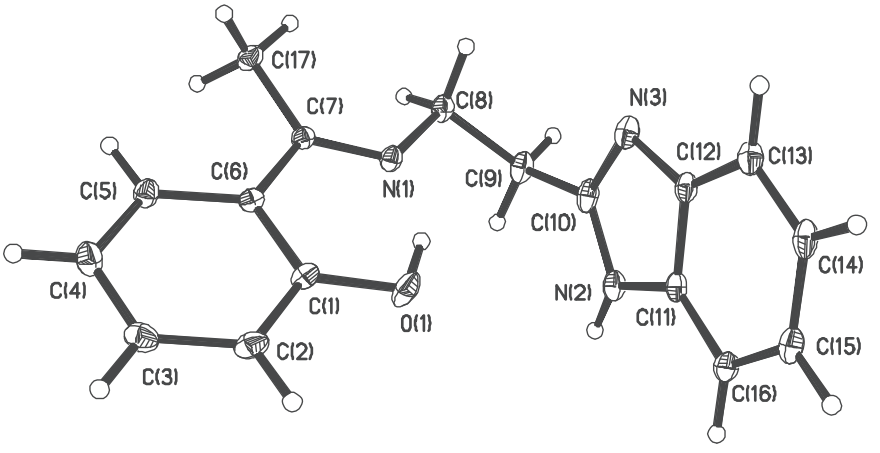

Figure 1. ORTEP plot of Hhap-aebmz. All non-hydrogen atoms are represented by their 30% probability ellipsoids. Hydrogens are included.

Table 2. Bond lengths (Å) and angles (°) for **I** and **1**.

I		**1**	
Bond lengths			
N(1)–C(7)	1.2852(16)	Cu(1)–O(1)	1.9293(15)
N(1)–C(8)	1.4590(16)	Cu(1)–N(1)	1.9549(18)
O(1)–C(1)	1.3446(16)	Cu(1)–N(2)	2.0511(17)
N(2)–C(10)	1.3372(18)	Cu(1)–Cl(1)	2.2480(6)
N(2)–C(11)	1.3889(16)	N(1)–C(7)	1.296(3)
N(3)–C(10)	1.3422(18)	N(1)–C(8)	1.474(3)
N(3)–C(12)	1.3870(17)	O(1)–C(1)	1.292(3)
Bond angles			
C(7)–N(1)–C(8)	122.69(11)	O(1)–Cu(1)–N(1)	91.44(7)
O(1)–C(1)–C(2)	117.98(11)	O(1)–Cu(1)–N(2)	143.96(7)
O(1)–C(1)–C(6)	122.05(11)	N(1)–Cu(1)–N(2)	89.74(7)
C(10)–N(2)–C(11)	106.11(11)	O(1)–Cu(1)–Cl(1)	92.41(5)
C(10)–N(3)–C(12)	105.91(11)	N(1)–Cu(1)–Cl(1)	161.36(5)
N(1)–C(7)–C(6)	117.06(11)	N(2)–Cu(1)–Cl(1)	97.75(5)
N(1)–C(7)–C(17)	123.91(11)	C(7)–N(1)–Cu(1)	128.47(15)
N(1)–C(8)–C(9)	108.55(10)	C(8)–N(1)–Cu(1)	108.92(13)
N(1)–C(7)–C(17)	123.91(11)	C(1)–O(1)–Cu(1)	126.50(13)
N(1)–C(8)–C(9)	108.55(10)	C(10)–N(2)–Cu(1)	124.52(14)
N(2)–C(10)–N(3)	113.10(12)	C(12)–N(2)–Cu(1)	127.77(13)

presented in table 2 (further details are provided in table S2 of Supplementary material). The difference of the current structure from the literature is existence as a supramolecule through hydrogen-bonding while other reported structures are dimeric where two chlorides bridge [4–8]. Strong intermolecular hydrogen-bonding exists between NH of benzimidazole and bonded phenolic oxygen (see table S1) as shown in figure S1 (see Supplementary material) and this is responsible for the supramolecular assembly. Short contacts between Cu–Cl and N–Cl of different complexes appear in the supramolecular structure (figure 4). The interaction between chloride and copper

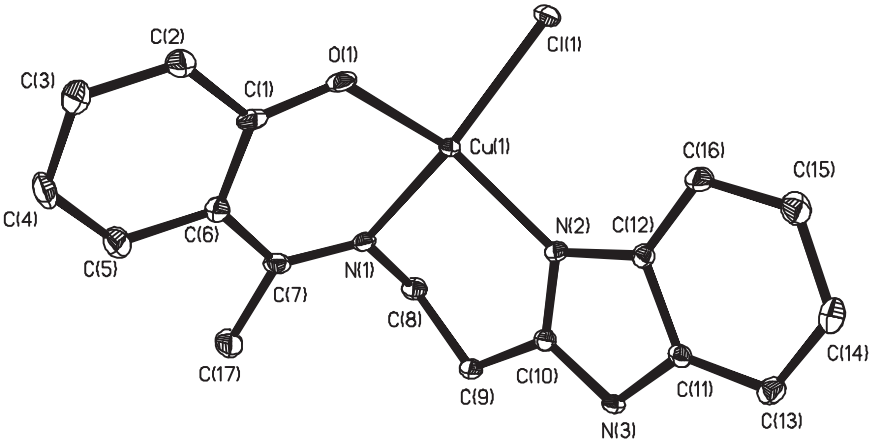

Figure 2. ORTEP plot of [Cu^{II}(hap-aebmz)Cl]. All non-hydrogen atoms are represented by their 50% probability ellipsoids. Hydrogens are omitted for clarity.

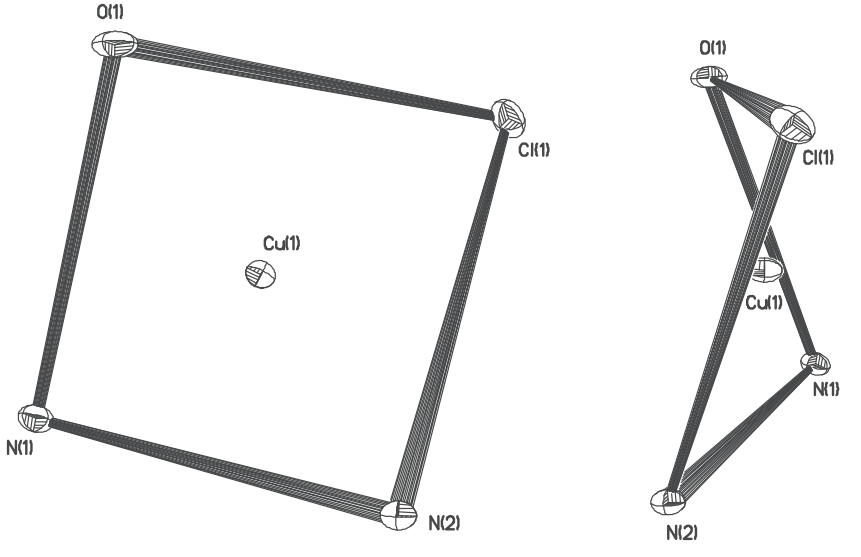

Figure 3. Coordination polyhedron around Cu(II) (two different views) in **1**.

of different complexes is weak [Cl(1)–Cu(1) : 2.974 Å)]. Chloride and nitrogen [Cl(1)–N(1): 3.258 Å] of different complexes have short contacts [17].

3.2. *IR spectral studies*

IR spectrum of **I** exhibits two sharp bands at 1615 and 1634 cm^{-1} due to υ(C=N) (azomethine/ring). These bands move to lower wavenumber (1610 cm^{-1}) on coordination of azomethine/ring nitrogen to copper. The presence of hydrogen bonds between

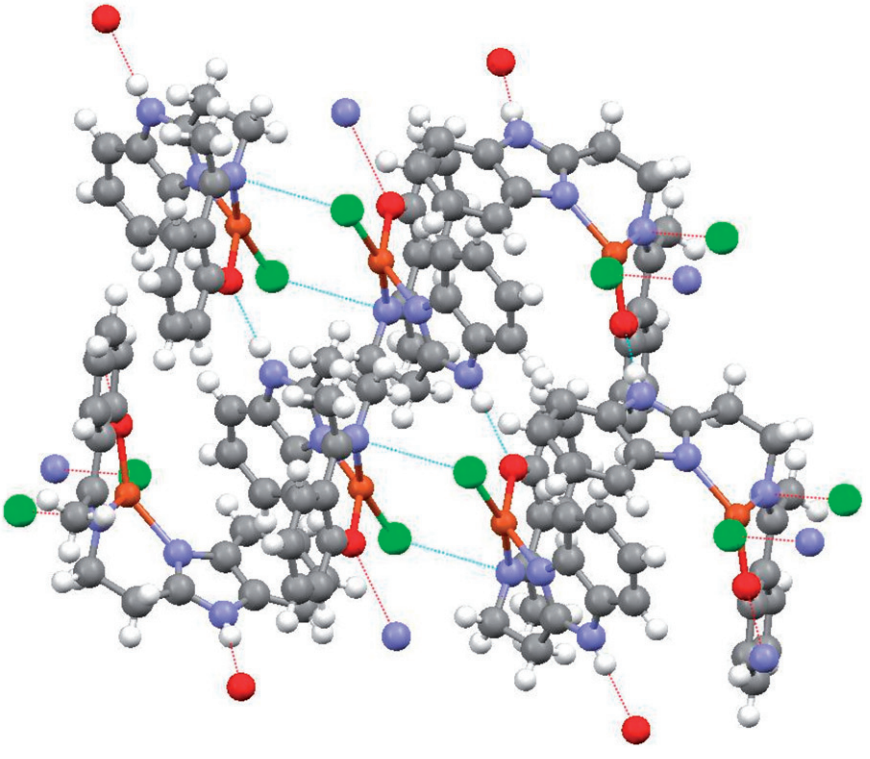

Figure 4. Crystal packing view of **1** with intermolecular hydrogen bonds between N(3)···O(1) and short contacts between Cl(1)–N(1).

NH of benzimidazole and other electronegative atoms in ligand is indicated by the appearance of several medium intensity bands at 2500–2700 cm^{-1}. These bands are also present in **1**, indicating the presence of hydrogen-bonding. The coordination of the phenolic oxygen could not be ascertained unequivocally due to the appearance of a weak band at *ca* 3400 cm^{-1}. However, structurally characterized complex, e.g., [VO_2(sal-aebmz)] (Hsal-aebmz = Schiff base derived from salicylaldehyde and 2-aminoethylbenzimidazole) [18] and [Cu^{II}(hap-aebmz)Cl] discussed in this article, confirms the monobasic tridentate ONN behavior of **I**. The far IR region for the complex exhibits three sharp bands at 570, 530, and 315 cm^{-1} due to υ(Cu–O), υ(Cu–N), and υ(Cu–Cl), respectively. Complex **2** exhibits these bands at 1612 cm^{-1} (C=N), 570 cm^{-1} (Cu–O), 455 cm^{-1} (Cu–N), and 315 cm^{-1} (Cu–Cl).

3.3. *Electronic spectral studies*

Table 3 presents electronic spectral data of ligand and complexes. The UV spectrum of the ligand is similar to that of Hsal-aebmz reported earlier [18]. All these bands are also present in **1** with slight variations. A band at 452 nm is assigned to the ligand-to-metal charge transfer (LMCT) from the phenolate oxygen to an empty d orbital of copper. A broad band at *ca* 700 nm also appears due to d–d transition of Cu^{II}. Encapsulated **2**

Table 3. Electronic spectral data (in nm) of **I** and **1**.

Compound	Solvent	λ_{max} (ε)[a]
Hhap-aebmz	MeOH	204(5839), 248(1575), 274(1539), 281(1498), 320(328), 388(251)
[Cu^{II}(hap-aebmz)Cl]	MeOH	212(2366), 235(1251), 271(912), 277(821)), 357(201), 299(198), 452(173), 700(47)
[Cu^{II}(hap-aebmz)Cl]-Y	Nujol	225, 297, 390, 500

[a]ε in L mol^{-1} cm^{-1}.

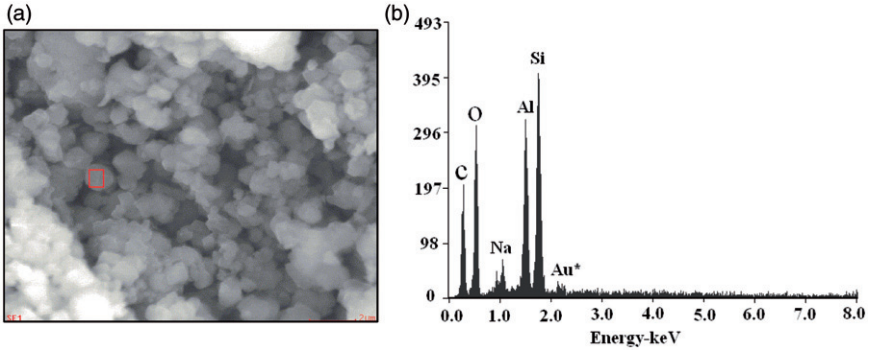

Figure 5. (a) SEM of [Cu^{II}(hap-aebmz)Cl]-Y and (b) EDX profile of [Cu^{II}(hap-aebmz)Cl]-Y.

displays only two bands at 225 and 297 nm in Nujol in the UV region and LMCT band at 500 nm in the visible region. The d–d transition band could not be located due to poor loading of **1** in the zeolite-Y.

3.4. *Field emission-scanning electron micrograph and EDX*

Accurate information on the morphological changes in terms of exact orientation of ligands coordinated to copper has not been possible due to poor loading of the metal complex. However, it is clear from the micrograph that zeolite-Y having encapsulated complex has well-defined crystals free from any shadow of the metal ions or complex present on its external surface. The micrograph of [Cu^{II}(hap-aebmz)Cl]-Y is presented in figure 5 along with the EDX profile. EDX plot, evaluated semi-quantitatively, supports this conclusion as no copper or nitrogen contents were noted on the spotted surface on the micrograph of [Cu^{II}(hap-aebmz)Cl]-Y. Thus, complex is present in the nano-cavities of the zeolite-Y.

3.5. *Powder X-ray diffraction study*

The powder X-ray diffraction patterns of Na-Y, [Cu^{II}]-Y, and [Cu^{II}(hap-aebmz)Cl]-Y (figure S2) were recorded at 2θ values between 5° and 70° to compare their crystalline nature and to ensure encapsulation of complex inside the cavity. Similar diffraction patterns in encapsulated complex, [Cu^{II}]-Y and Na-Y were noticed except a slightly

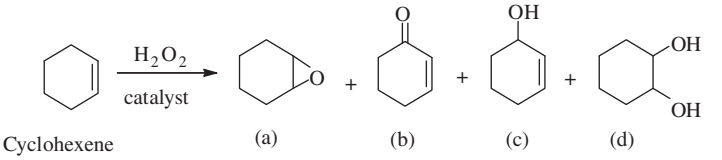

Scheme 2. Reaction products of cyclohexene oxidation. (a) = cyclohexene epoxide, (b) = 2-cyclohexene-1-one, (c) = 2-cyclohexene-1-ol, and (d) = cyclohexane-1,2-diol.

weaker intensity of the zeolite having metal complex encapsulated. These observations indicate that the framework of zeolite has not undergone any significant structural change during incorporation of the catalyst, i.e., crystallinity of the zeolite-Y is preserved during encapsulation. No new peaks due to encapsulated complex were detected in the complex encapsulated sample, possibly due to very low percentage loading of metal complex. However, the copper content found (see section 2) after encapsulation is only due to the presence of copper(II) complex in the cavities of the zeolite-Y.

3.6. *Catalytic reactions*

3.6.1. Oxidation of cyclohexene. [Cu^{II}(hap-aebmz)Cl]-Y catalyzes oxidation of cyclohexene by H_2O_2 efficiently to give cyclohexene epoxide, 2-cyclohexene-1-one, 2-cyclohexene-1-ol, and cyclohexane-1,2-diol as presented in scheme 2.

Reaction conditions have been optimized for maximum oxidation of cyclohexene by varying different parameters, namely the amount of oxidant (moles of H_2O_2 per mole of cyclohexene), catalyst (amount of catalyst per mole of cyclohexene), temperature, and amount of solvent.

Three different cyclohexene to aqueous 30% H_2O_2 molar ratios, namely 1 : 1, 1 : 2, and 1 : 3 were considered while keeping fixed amounts of cyclohexene (0.82 g, 10 mmol) and catalyst (0.004 g) in 10 mL of MeCN and the reaction was carried out at 80°C. The percentage conversion of cyclohexene as a function of time is presented in figure 6. A maximum of 85.0% conversion was obtained at a cyclohexene/aqueous H_2O_2 molar ratio of 1 : 1 in 6 h reaction. This conversion reached 91.0% and 95.0% at cyclohexene/H_2O_2 ratio of 1 : 2 and 1 : 3, respectively. As cyclohexene/aqueous H_2O_2 ratio of 1 : 3 showed an increment of only 4% as compared to that of 1 : 2, a 1 : 2 molar ratio was considered suitable to obtain the optimum cyclohexene conversion of 91.0% in 6 h reaction.

The effect of amount of catalyst on oxidation of cyclohexene is shown in figure 7. Three different amounts of catalyst, namely 0.003, 0.004, and 0.005 g were considered while keeping fixed amount of cyclohexene (0.82 g, 10 mmol), aqueous H_2O_2 (2.27 g, 20 mmol) in MeCN (10 mL); the reaction was carried out at 80°C. It is clear from the plot that 0.005 g catalyst gives the highest conversion (96%) of cyclohexene.

Figure S3 illustrates the oxidation of cyclohexene at three different volumes (5, 10, and 15 mL) while keeping optimized conditions of catalyst (0.005 g), cyclohexene (0.82 g, 10 mmol), and H_2O_2 (2.27 g, 20 mmol), and running the reaction at 80°C. It is evident from the plot that the performance of the reaction in 5 mL solvent is suitable to obtain nearly quantitative oxidation (99.6%) of cyclohexene. Similarly, we have also

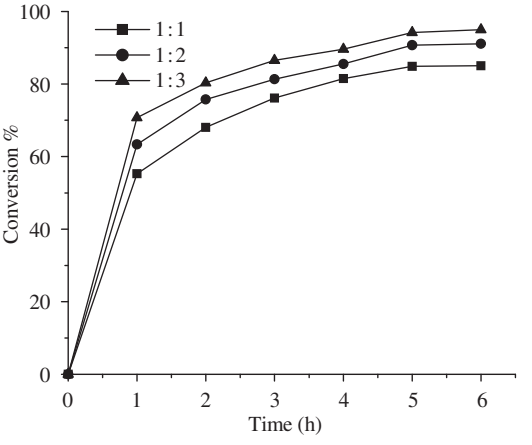

Figure 6. Effect of oxidant concentration on cyclohexene oxidation. Reaction conditions: cyclohexene (0.82 g, 10 mmol), catalyst (0.004 g), acetonitrile (10 mL), and temperature (80°C).

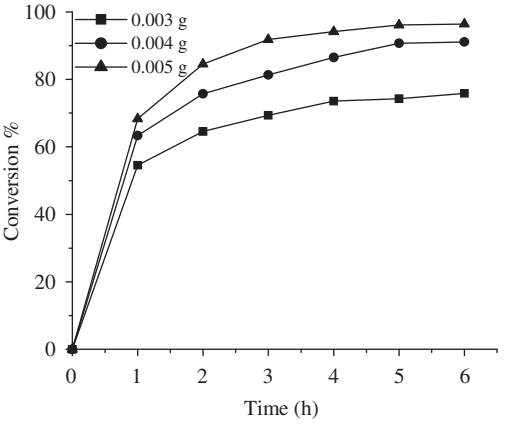

Figure 7. Effect of catalyst amount on the cyclohexene oxidation. Reaction conditions: cyclohexene (0.82 g, 10 mmol), H_2O_2 (2.27 g, 20 mmol), acetonitrile (10 mL), and temperature (80°C).

observed that conducting the catalytic reaction at 80°C is most suitable to maximize the oxidation of cyclohexene.

Thus, for the maximum oxidation of 10 mmol (0.82 g) of cyclohexene, the other required conditions are: [Cu^{II}(hap-aebmz)Cl]-Y (0.005 g), H_2O_2 (2.27 g, 20 mmol), acetonitrile (5 mL), and temperature (80°C). Under these conditions nearly quantitative oxidation (99.6%) of cyclohexene was achieved with selectivity of different products in the order: 2-cyclohexene-1-ol (44%) > 2-cyclohexene-1-one (40%) cyclohexene epoxide (12%) > cyclohexane-1,2-diol (4%). A maximum of 90% conversion with neat catalyst precursor [Cu^{II}(hap-aebmz)Cl] was obtained under similar conditions where product selectivity varied in the order: 2-cyclohexene-1-ol (33%) > 2-cyclohexene-1-one (32%) > cyclohexane-1,2-diol (23%) > cyclohexene epoxide (8%). Thus, encapsulated catalyst performs better in catalyzing oxidation of cyclohexene almost quantitatively.

Catalytic potential of the encapsulated complex presented here compares well with similar encapsulated complexes. For example, [Cu(2-pyrazinecarboxylate)$_2$]-Y exhibited as high as 90.5% conversion of cyclohexene at a substrate to oxidant (30% H_2O_2) ratio of 1 : 2 where no formation of cyclohexene epoxide was observed and the selectivity of the other oxidation products varied in the order: 2-cyclohexene-1-one (51%) > 2-cyclohexene-1-ol (42.4%) > cyclohexane-1,2-diol (6.6%) [19]. [Cu(sal-oaba)(H_2O)]-Y, however, exhibited only 45.8% conversion with the formation of only two products, 2-cyclohexene-1-one and 2-cyclohexene-1-ol [20]. Cyclohexene was oxidized very slowly by *tert*-butylhydroperoxide using similar catalyst [Cu(pan)Cl)]-Y (where Hpan = 1-(2-pyridylazo)-2-naphthol) under aerobic conditions and only 28% conversion was obtained with selectivity of products in the order: 1-*tert*-butylperoxy-2-cyclohexene 89% > 2-cyclohexene-1-one (11%) [21].

The reaction mixture of [Cu^{II}(hap-aebmz)Cl]-Y, cyclohexene and solvent under optimized conditions after a contact time of 6 h at 80°C was filtered and after activating the catalyst by washing with acetonitrile and drying at *ca.* 120°C, it was subjected to further catalytic reaction under similar conditions. A maximum conversion of 98% suggests that complex is still present in the cavity of the zeolite-Y. The filtrate collected after separating the used catalyst was placed into the reaction flask and the reaction was continued after adding fresh oxidant for another 2 h. The gas chromatographic analysis showed no change in conversion, and this confirms that the reaction did not proceed upon removal of the solid catalyst. The reaction was, therefore, heterogeneous in nature.

3.6.2. Oxidation of phenol. Catalysts based on ZEMC have played a role in oxidation of phenol with a wide range of product selectivity reported [22–24]. Oxidation of phenol catalyzed by [Cu^{II}(hap-aebmz)Cl]-Y using H_2O_2 as oxidant gave catechol and hydroquinone with a mass balance of *ca* 97%. These are the only expected products based on phenol. Gas chromatographic analysis also indicated a minor product, which may possibly be benzoquinone formed by partial oxidation of hydroquinone (scheme 3) but it was ignored. Slight coloration of reaction mixture, which is not detectable by GC under the conditions used herein, is possibly due to polymeric materials.

In order to achieve suitable reaction conditions for maximum oxidation of phenol, (i) amount of catalyst per mole of phenol, (ii) H_2O_2 concentration (moles of H_2O_2 per mole of phenol, (iii) volume of solvent, and (iv) temperature of the reaction mixture were also studied here.

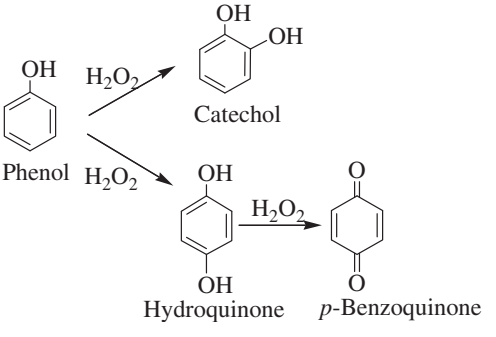

Scheme 3. Reaction products of phenol oxidation.

The effect of amount of catalyst on the oxidation of phenol is shown in figure 8. Increasing the catalyst amount from 0.005 to 0.010 g at fixed amount of phenol (1.88 g, 20 mmol), aqueous 30% H_2O_2 (2.27 g, 20 mmol), acetonitrile (5 mL), and temperature (80°C) increases the conversion from 40.3% to 43.3%. Further increasing the catalyst amount to 0.015 g initiates the reaction quickly but overall conversion of phenol reaches to only 37.1%. As 0.010 g catalyst shows only 3% increment of conversion compared to 0.005 g of catalyst, an amount of 0.005 g is considered the best.

Using three different phenols to H_2O_2 molar ratios, namely 1 : 1, 1 : 2, and 1 : 3 for a fixed amount of phenol (1.88 g, 20 mmol), [Cu^{II}(hap-aebmz)Cl]-Y (0.005 g), MeCN (5 mL), and temperature (80°C), the obtained percentage conversion of phenol were 40.3%, 48.3%, and 65.7%, respectively. It is clear from the plot presented as a function of time (figure 9) that the phenol to aqueous 30% H_2O_2 molar ratio of 1 : 3 is the best ratio to obtain maximum oxidation of phenol (65.7%) at 80°C while 1 : 1 and 1 : 2 molar ratios gave lower conversions. About 6 h was required to establish the equilibrium.

Variation in the volume of the solvent was studied by taking 5, 10, and 15 mL of acetonitrile (figure S4). For 1.88 g (20 mmol) of phenol, catalyst (0.005 g), H_2O_2 (7.98 g, 60 mmol), acetonitrile (5 mL), and reaction temperature (80°C) gave good transformation (65.7%) of phenol. The temperature of the reaction medium also influences the reaction rate. It was inferred that 80°C was the best suited temperature for the maximum oxidation of phenol under the above reaction conditions. At this temperature, a maximum of 65.7% conversion of phenol was achieved in 6 h. Lowering the temperature lowers the conversion of phenol. Catalytic results under all reaction conditions are presented in table 4.

Thus, optimized operating reaction conditions for maximum oxidation of phenol were: phenol (1.88 g, 20 mmol), [Cu^{II}(hap-aebmz)Cl]-Y (0.005 g), 30% H_2O_2 (6.81 g, 60 mmol), acetonitrile (5 mL), and reaction temperature (80°C). Under these conditions, [Cu^{II}(hap-aebmz)Cl]-Y exhibits 65.7% conversion with selectivity of major product, catechol of 66.1% and hydroquinone of 32.9%. The performance of the neat complex [Cu^{II}(hap-aebmz)Cl], considering same mole concentration as was used for encapsulated one, under the above reaction conditions is low (44%) with 66% selectivity of the major product. Thus, encapsulation of the complex [Cu^{II}(hap-aebmz)Cl] in zeolite-Y

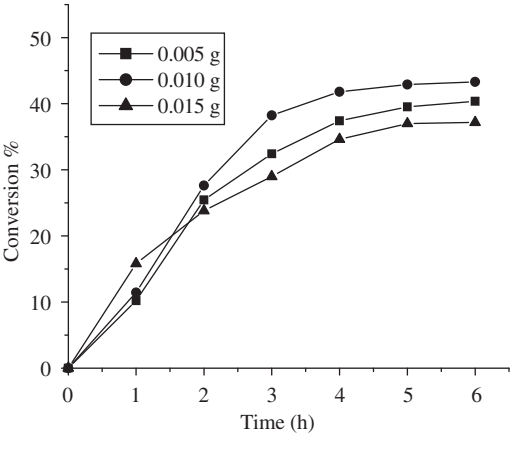

Figure 8. Effect of catalyst amount on phenol oxidation. Reaction conditions: Phenol (1.88 g, 20 mmol), H_2O_2 (2.27 g, 20 mmol), acetonitrile (5 mL), and temperature (80°C).

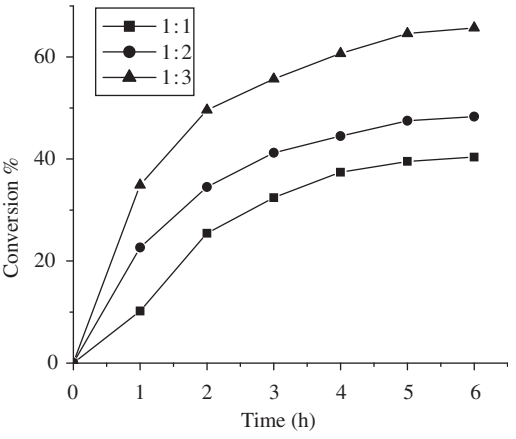

Figure 9. Effect of oxidant concentration on phenol oxidation. Reaction conditions: phenol (1.88 g, 20 mmol), catalyst (0.005 g), acetonitrile (5 mL), and temperature (80°C).

Table 4. Conversion of phenol (1.88 g, 20 mmol) using [Cu^{II}(hap-aebmz)Cl]-Y as catalyst in 6 h of reaction time under different reaction conditions.

Catalyst (g)	H_2O_2 (g, mmol)	Temperature (°C)	MeCN (mL)	Conversion (%)	Selectivity (%)		
					Cat	Hq	Unidentified
0.005	2.27, 20	80	5	40.3	70.6	27.0	2.4
0.010	2.27, 20	80	5	43.3	60.1	36.5	3.4
0.015	2.27, 20	80	5	37.2	69.7	29.9	0.4
0.005	4.54, 40	80	5	48.3	66.7	32.3	1.0
0.005	6.81, 60	80	5	65.7	66.1	32.9	1.0
0.005	6.81, 60	80	10	65.4	66.6	33.2	0.2
0.005	6.81, 60	80	15	60.1	66.4	33.5	0.1
0.005	6.81, 60	75	5	62.9	67.2	32.8	–

enhances its catalytic activity. The overall performance of encapsulated complex also gives higher turnover frequency than the corresponding neat one.

The catalytic performance of the encapsulated complex reported here is better than the data reported in the literature. For example, the observed conversions for zeolite-Y encapsulated complexes are: [Cu(sal-ambmz)Cl]-Y (42.0%) [9], [Cu(salpn)]-Y (H_2salpn = N,N′-bis(salicylidene)propane-1,3-diamine) (31%) [25], Cu(saldien)]-Y (46%) [26], and [VO(salen)]-Y (32.6%) [27]. Catalyst NH_4[VO(sal-inh)]-Y (H_2sal-inh = Schiff base derived from salicylaldehyde and isonicotinic acid hydrazide) exhibits only 26.5% conversion [28]. The selectivity toward the formation of catechol in all cases is always higher than hydroquinone.

3.7. *Reaction of [Cu^{II}(hap-aebmz)Cl] with H_2O_2 and possible reaction pathway of the catalyst*

At least three types of intermediates having a copper–oxygen interaction, namely side-on Cu^{III}–(μ-η^2-peroxido)–Cu^{III}, bis(μ-oxido–Cu^{III}), and Cu^{III}–O–O–H

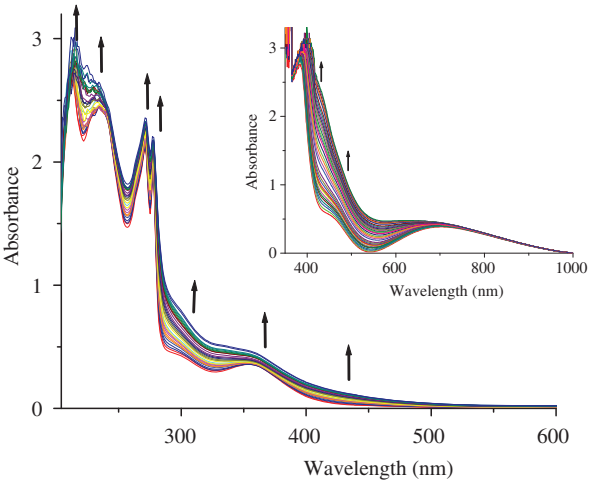

Figure 10. Spectral changes observed during titration of a methanolic solution of [Cu^{II}(hap-aebmz)Cl] (*ca* 10^{-4} mol L^{-1}) with 30% H_2O_2 dissolved in minimum amount of methanol. Spectra were recorded after successive addition of 2 drops of H_2O_2 solution. Inset shows similar titration with higher concentration of complex (*ca* 10^{-3} mol L^{-1}).

(copperhydroperoxide) have been reported during the catalytic action [29, 30]. We have studied the interaction of **1** with H_2O_2 in methanol by electronic absorption spectroscopy to identify possible intermediates during catalytic activity. Addition of one-drop portions of 30% H_2O_2 dissolved in methanol to *ca* 10^{-3} mol L^{-1}methanolic solution of [Cu^{II}(hap-aebmz)Cl] results in gradual weakening of the 700 nm band. The band at 452 nm also weakens along with increasing intensity and shifting to *ca* 445 nm (see inset of figure 10). Addition of H_2O_2 to a diluted solution (*ca* 10^{-4} M) resulted in increasing intensities of 357 and 299 nm bands (figure 10) along with their conversion into weak shoulders. Two bands at 271 and 277 nm remain almost unchanged while bands at 212 and 235 nm slightly gain intensity. All these suggest interaction of H_2O_2 with Cu^{II}. As [Cu^{II}(hap-aebmz)Cl] is expected to remain monomeric in the nano-cavity of zeolite-Y, facile formation of [(HOO)-Cu^{III}(hap-aebmz)Cl] is expected because of its possibility to expand coordination number even in the cavity of zeolite-Y. Expansion of coordination number of Cu^{II} complexes having monobasic tridentate ONN donors through dimerization/polymerization is very common [4–8]. Such (L)Cu^{III}–O–O–H complexes exhibit a charge transfer band at *ca* 600 nm [31]. The decrease in the intensity of 700 nm band without any isosbestic point may be due to merging of this additional charge transfer band with the d–d transition. The peroxide intermediate finally transfers coordinated oxygen to the substrate to give the products.

4. Conclusion

By using the Schiff base Hhap-aebmz, an ONN donor, [Cu^{II}(hap-aebmz)Cl], has been prepared. Structures of ligand and complex have been confirmed by single crystal X-ray study. [Cu^{II}(hap-aebmz)Cl] has been encapsulated in the cavity of zeolite-Y and its

catalytic activity for oxidation of cyclohexene is evaluated. Nearly quantitative conversion with selectivity in the order 2-cyclohexene-1-ol (44%) > 2-cyclohexene-1-one (40%) > cyclohexene epoxide (12%) > cyclohexane-1,2-diol (4%) has been obtained. The recyclability of the catalyst is an added advantage. Oxidation of cyclohexene proceeds through intermediate [(HOO)-Cu^{III}(hap-aebmz)Cl] species, formation of which has been demonstrated by electronic absorption spectroscopy.

Supplementary material

CCDC Nos 813836 (Hhap-aebmz, **I**) and 813837 ([Cu^{II}(hap-aebmz)Cl], **1**) contain the supplementary crystallographic data for this article. These data can be obtained free of charge from the Cambridge Crystallographic Data Centre *via* www.ccdc.cam.ac.uk/data_request/cif.

Acknowledgments

The authors are grateful to the Council of Scientific and Industrial Research, New Delhi, for financial assistance.

References

[1] R. Vicente, A. Escuer, E. Peñalba, X. Solans, M. Font-Bardía. *J. Chem. Soc., Dalton Trans*., 3005 (1994).
[2] A. Escuer, M. Font-Bardia, E. Penñalba, X. Solans, R. Vicente. *Inorg. Chim. Acta*, **286**, 189 (1999).
[3] C.R. Choudhury, S.K. Dey, R. Karmakar, C.-D. Wu, C.-Z. Lu, M.S. El Fallah, S. Mitra. *New J. Chem*., **27**, 1360 (2003).
[4] P. Talukder, A. Datta, S. Mitra, G. Rosair, M.S. El Fallah, J. Ribas. *Dalton Trans*., 4161 (2004).
[5] S.K. Dey, N. Mondal, M.S. El Fallah, R. Vicente, A. Escuer, X. Solans, M. Font-Bardía, T. Matsushita, V. Gramlich, S. Mitra. *Inorg. Chem*., **43**, 2427 (2004).
[6] S. Sen, P. Talukder, S.K. Dey, S. Mitra, G. Rosair, D.L. Hughes, G.P.A. Yap, G. Pilet, V. Gramlich, T. Matsushita. *Dalton Trans*., 1758 (2006).
[7] S. Basak, S. Sen, S. Banerjee, S. Mitra, G. Rosair, M.T.G. Rodríguez. *Polyhedron*, **26**, 5104 (2007).
[8] S. Basak, S. Sen, C. Marschner, J. Baumgartner, S.R. Batten, D.R. Turner, S. Mitra. *Polyhedron*, **27**, 1193 (2008).
[9] M.R. Maurya, A.K. Chandrakar, S. Chand. *J. Mol. Catal. A: Chem*., **263**, 227 (2007).
[10] G.S. Rafelt, J.H. Clark. *Catal. Today*, **57**, 3 (2000), and references therein.
[11] R.A. Sheldon, I.W.C.E. Arends, A. Dijksman. *Catal. Today*, **57**, 157 (2000).
[12] C.R. Jacob, S.P. Verkey, P. Ratnasamy. *Microporous Mesoporous Mater*., **22**, 465 (1998).
[13] G.J. Hutchings. *Chem. Commun*., 301 (1999).
[14] M.R. Maurya, S.J.J. Titinchi, S. Chand. *J. Mol. Catal. A: Chem*., **214**, 257 (2004).
[15] M.R. Maurya, A. Kumar, J. Costa Pessoa. *Coord. Chem. Rev*., **255**, 2315 (2011).
[16] G.M. Sheldrick. *SHELXL-97: An Integrated System for Solving and Refining Crystal Structures from Diffraction Data (Revision 5.1)*, University of Göttingen, Germany (1997).
[17] J.P.M. Lommerse, A.J. Stone, R. Taylor, F.H. Allen. *J. Am. Chem. Soc*., **118**, 3108 (1996).
[18] M.R. Maurya, A. Kumar, M. Ebel, D. Rehder. *Inorg. Chem*., **45**, 5924 (2006).
[19] P. Chutia, S. Kato, T. Kojima, S. Satokawa. *Polyhedron*, **28**, 370 (2009).
[20] M.R. Maurya, A.K. Chandrakar, S. Chand. *J. Mol. Catal. A: Chem*., **274**, 192 (2007).
[21] I. Kuźniarska-Biernacka, K. Biernacki, A.L. Magalhães, A.M. Fonseca, I.C. Neves. *J. Catal*., **278**, 102 (2011).
[22] R. Raja, P. Ratnasamy. *Stud. Surf. Sci. Catal*., **101**, 181 (1996).

[23] S. Seelan, A.K. Sinha, D. Srinivas, S. Sivasanker. *Bull. Catal. Soc. India*, **1**, 29 (2002).
[24] K.J. Balkus Jr, A.G. Gabrielov. *J. Incl. Phenom. Mol. Recog. Chem.*, **21**, 159 (1995).
[25] M.R. Maurya, S.J.J. Titinchi, S. Chand. *Appl. Catal. A: Gen.*, **228**, 177 (2002).
[26] M.R. Maurya, S.J.J. Titinchi, S. Chand. *J. Mol. Catal. A: Chem.*, **201**, 119 (2003).
[27] M.R. Maurya, M. Kumar, S.J.J. Titinchi, H.S. Abbo, S. Chand. *Catal. Lett.*, **86**, 97 (2003).
[28] M.R. Maurya, H. Saklani, A. Kumar, S. Chand. *Catal. Lett.*, **93**, 121 (2004).
[29] E.I. Solomon, P. Chen, M. Metz, S.-K. Lee, A.E. Palner. *Angew. Chem. Int. Ed.*, **40**, 4570 (2001).
[30] J.P. Klinman. *Chem. Rev.*, **96**, 2541 (1996).
[31] K.D. Karlin, J.C. Hayes, Y. Gultneh, R.W. Cruse, J.W. McKown, J.P. Hutchinson, J. Zubieta. *J. Am. Chem. Soc.*, **106**, 2121 (1984).